nature chemistry

Article

https://doi.org/10.1038/s41557-023-01362-3

Modular and diverse synthesis of amino acids via asymmetric decarboxylative protonation of aminomalonic acids

Received: 14 February 2023

Accepted: 6 October 2023

Check for updates

Wei-Feng Zheng [1], Jingdan Chen [2], Xiaotian Qi [2] ✉ & Zhongxing Huang [1] ✉

Stereoselective protonation is a challenge in asymmetric catalysis. The small size and high rate of transfer of protons mean that face-selective delivery to planar intermediates is hard to control, but it can unlock previously obscure asymmetric transformations. Particularly, when coupled with a preceding decarboxylation, enantioselective protonation can convert the abundant acid feedstocks into structurally diverse chiral molecules. Here an anchoring group strategy is demonstrated as a potential alternative and supplement to the conventional structural modification of catalysts by creating additional catalyst–substrate interactions. We show that a tailored benzamide group in aminomalonic acids can help build a coordinated network of non-covalent interactions, including hydrogen bonds, π–π interactions and dispersion forces, with a chiral acid catalyst. This allows enantioselective decarboxylative protonation to give α-amino acids. The malonate-based synthesis introduces side chains via a facile substitution of aminomalonic esters and thus can access structurally and functionally diverse amino acids.

Face-selective addition to planar substrates or intermediates is one of the fundamental modes of asymmetric catalysis. Among asymmetric transformations that can be enabled by this paradigm, C–H bond formation via protonation offers a straightforward approach to generate tertiary stereocentres that are prevalent in biomolecules[1–3]. Moreover, when planar intermediates generated from decarboxylation were intercepted by an enantioselective proton transfer, it was shown that the decarboxylative protonation can bridge the easily available carboxylic acids and structurally diverse chiral molecules (Fig. 1a)[4]. However, the challenges associated with the enantiocontrol of asymmetric decarboxylation are daunting. Besides the inherent difficulty arising from the small size of the hydrogen atom and potential racemization of the product, the acidic nature of the decarboxylation reactants entails a catalytic pathway that is kinetically favoured over the background protonation that gives racemic products.

Central to the face selectivity of proton transfer is the catalyst–substrate interaction that fixes the orientation of planar substrates or intermediates. These favoured conformations are often organized with catalysts at the reaction site utilizing distinct interaction modes (Fig. 1b). While metal complexes are frequently used to generate chiral enolates as proton acceptors[5–7], transfers between chiral proton donors and achiral acceptors are often enabled by ion-pairing[8–11] or enzymatic catalysis[12,13]. Nevertheless, these interactions are often confined in the proximity of the protonation site. Their stabilization effects still fall short of coupling CO_2 extrusion with a fast and stereoselective protonation to enable a general asymmetric decarboxylation of carboxylic acids.

In this Article, an anchoring group strategy is proposed to enhance the enantiocontrol via a dual-site mode of interactions (Fig. 1c). We envision that besides the primary interactions at the reaction site, a tailored and ideally removable functional group on the substrate can create secondary interactions with the catalyst at a different location. In the case of asymmetric decarboxylation, it is proposed that while a chiral Brønsted acid[14–17] interacts with the π bond of the enol intermediate during the proton transfer, a pendant substituent (the anchoring

[1]State Key Laboratory of Synthetic Chemistry, Department of Chemistry, The University of Hong Kong, Hong Kong, China. [2]College of Chemistry and Molecular Sciences, Wuhan University, Wuhan, China. ✉e-mail: qi7xiaotian@whu.edu.cn; huangzx@hku.hk

https://doi.org/10.1038/s41557-023-01362-3

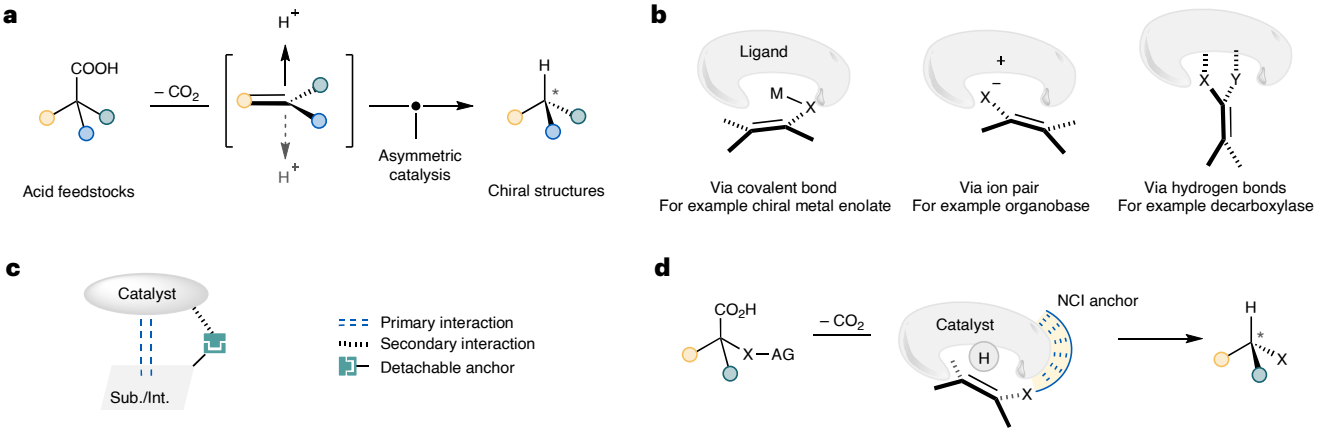

Fig. 1 | Anchoring group strategy for asymmetric decarboxylative protonation. a, Stereoselective decarboxylative protonation. Inducing enantioselectivity of a decarboxylation reaction is a daunting challenge in catalysis, as the face selectivity of protonating the planar intermediates is difficult to control. However, these asymmetric decarboxylation transformations hold great promise for converting easily available carboxylic acids into valuable chiral building blocks. **b**, Established modes of face selectivity control. Conventional modes of catalysis control the face selectivity of proton transfer by fixing the conformation of planar intermediates in the proximity of the protonation site. For example, a metal complex is employed to form a metal enolate and enantiocontrol is imposed using its chiral ligand. Non-covalent interactions are used as well, as exemplified in ion-pairing and enzymatic catalysis, by electrostatic forces and hydrogen bonds, respectively. Nevertheless, these interactions are often inadequate to create a fast and selective protonation that can be coupled with a preceding decarboxylation. **c**, Dual-site mode of interactions between the catalyst and substrate (Sub.) or intermediate (Int.). In addition to the reaction site, an attached functional group on the substrate/intermediate is expected to create additional stabilization by interacting with the catalyst at a different site (for example the catalyst backbone). **d**, Proposed asymmetric decarboxylation facilitated by a non-covalent interaction anchor. In our proposal, while a chiral Brønsted acid catalyst and the enol intermediate undergo a proton transfer around the acid motif, an anchoring group on the substituent of the enol is expected to induce multiple non-covalent interactions with the backbone of the acid catalyst, including hydrogen bonds, π–π interactions and dispersion forces. NCI, non-covalent interaction; AG, anchoring group.

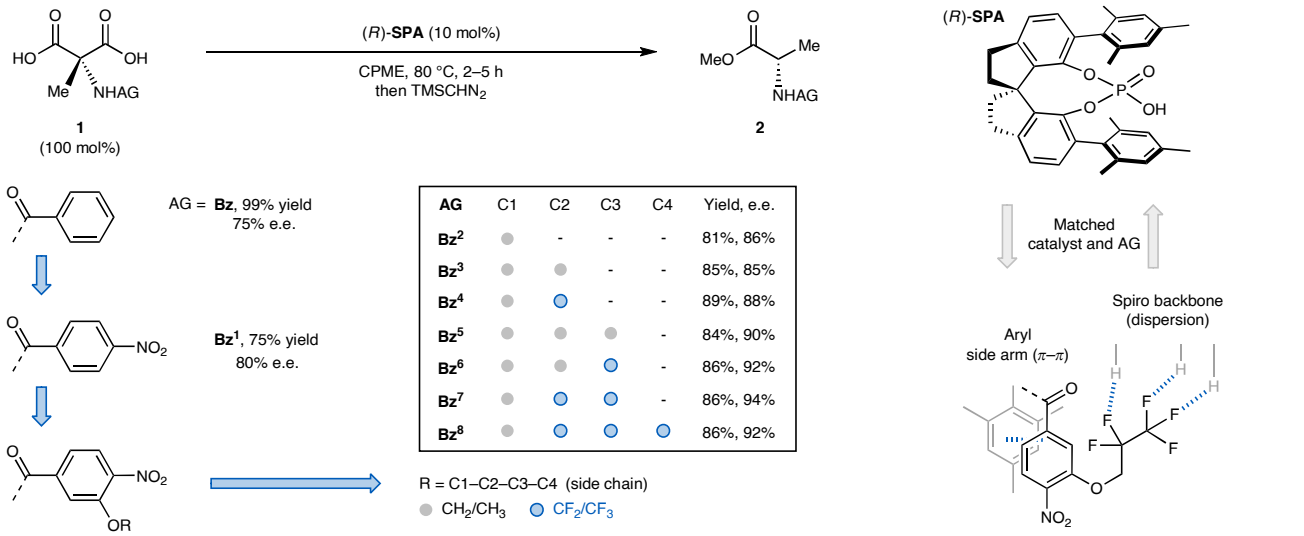

Fig. 2 | Identification and optimization of a benzamide non-covalent interaction anchor. Chiral phosphoric acids can catalyse the asymmetric decarboxylation of aminomalonic acids, albeit with a limitation in enantioselectivity. As proposed, the amine anchoring group can provide another handle for optimizing the enantiocontrol. It is found that the incorporation of a *para*-nitro and a *meta*-methoxy group (**Bz²**) can enhance the enantioselectivity significantly, presumably by making the amide motif a better hydrogen-bond donor and/or creating a π–π interaction between the electron-deficient arene and the mesityl side arm of **SPA**. Further improvement was obtained when the methoxy group was replaced with a polyfluoro alkoxy chain, particularly a pentafluoropropoxy group (**Bz⁷**). The benefits of these fluorinated alkyl chains may be attributed to their dispersion forces with the C–H-rich backbone of the phosphoric acid. SPA, spirocyclic phosphoric acid; Bz, benzoyl; CPME, cyclopentyl methyl ether.

group) of the olefinic intermediate could dock at the backbone of the acid in return to further affix the couple (Fig. 1d). It is also hypothesized that attractive non-covalent interactions, including π–π stacking and dispersion forces, are good candidates for these secondary interactions, as they are known to hold molecules together in a precise manner when working collectively[18,19]. Meanwhile, the weak nature of these forces is not expected to interrupt the primary interactions at the protonation site. However, manipulating and organizing various types of non-covalent interaction in a coordinated fashion is not an easy task.

To examine our hypothesis, we selected the asymmetric decarboxylation of aminomalonic acids to amino acids as a model reaction, as the amino motif is an ideal test ground for anchoring groups that can be readily installed and detached (Fig. 2)[20]. While carbonyl-derived protecting groups of amines, such as amides and carbamates, can act as

hydrogen-bond donors and/or acceptors, a diverse collection of motifs, such as substituted arenes and functionalized alkyl chains, can be easily attached and optimized to induce weak interactions. The synthetic value of the decarboxylation is significant as well, as it would enable a malonate-based synthesis of chiral amino acids where their side chains can be attached via the facile alkylation of aminomalonic esters (see below, Fig. 3). However, previous attempts at the decarboxylative synthesis of chiral amino acids via enzymatic[21] and organobase[22] catalysis were largely unsuccessful (Supplementary Fig. 1).

Results and discussion

Identifying and optimizing the anchoring group

An exhaustive examination of chiral phosphoric acids (Supplementary Fig. 2) for the asymmetric decarboxylation of malonic acid **1** to benzoylalanine **2** did reveal a limitation of enantiocontrol, with spirocyclic **SPA** giving the best, yet a moderate, enantioselectivity (Fig. 2)[23–25]. As proposed, enhancements in enantioselectivity were obtained by the optimization of the amine anchoring group, indicating its engagement with the chiral phosphoric acid during the enantioinduction. Benzamide (Bz) was revealed to be a preferred choice compared with other protecting groups, including acetyl, pivalate and benzyl carbamate (Supplementary Fig. 5). Its aromatic ring can offer a further handle for structural modification to enhance non-covalent interactions. Indeed, a *para*-nitro group (**Bz**^{1}) and a *meta*-methoxy group (**Bz**^{2}) on the ring could join forces to improve the enantioselectivity. Both substituents can enhance the acidity of the amide proton, which in return may act as a stronger hydrogen-bond donor to strengthen substrate–catalyst interaction. Meanwhile, the electron-deficient arene can also interact with a mesityl side arm of **SPA** via π–π stacking. Next, we considered it geometrically possible that an extended side chain of the *meta*-alkoxyl group could further help anchor the enol intermediate. Although simple elongation of the alkyl chain is only negligibly beneficial (**Bz**^{3} and **Bz**^{5}), the incorporation of multiple fluorides (**Bz**^{4} and **Bz**^{6}–**Bz**^{8}) raised the enantiocontrol to an excellent level, with the pentafluoropropoxy group (**Bz**^{7}) as the optimal substituent. The final and critical increment of enantiocontrol by the fluorinated chain is proposed to originate from its dispersive interaction with the C–H bond-rich skeleton of the phosphoric acid that serves as an additional anchor to fix the conformation of the enol.

Scope of the asymmetric malonic ester synthesis

Aminomalonic acids bearing the customized anchoring group (**Bz**^{7}) can be prepared in a divergent and modular fashion (Fig. 3). Starting from the inexpensive aminomalonate hydrochloride **3**, a hectogram-scale benzoyl installation to **4** as a common intermediate followed by the unified alkylation and hydrolysis conditions, can generate structurally diverse diacids for decarboxylation. The detachment of the anchoring group is equally facile. When a larger-scale decarboxylation under a lower catalyst loading was followed by hydrolytic work-up, analytically pure alanine salt (**5**) can be obtained by a simple extraction. This protocol also allows the recovery of the parent acid (**Bz**^{7}OH) of the anchoring group and phosphoric acid catalyst that remain in the organic phase (Supplementary Fig. 7). We note that while reducing the **SPA** loading decreases the enantioselectivity (Supplementary Fig. 6), slow addition of substrates can revive the enantiocontrol, presumably by lowering the concentration of the achiral proton source (that is aminomalonic acid) to inhibit the background protonation that gives racemic amino acids. Meanwhile, the commercial availability of **SPA** of opposite configurations allows access to both natural and unnatural enantiomers of amino acids, such as alanine derivatives (+)/(−)-**6**.

Structurally distinct amino acids have unique functions and our method can prepare a diversity of them. The chiral phosphoric acid can accommodate extended alkyl chains (**7**–**10**) and cycloalkyl (**11**) groups to generate unnatural amino acids, including those isomeric to proteinogenic ones, such as norvaline (**8**) and norleucine (**9**). The approach also tolerates more crowded secondary alkyl substituents (**12**), albeit with slightly reduced enantioselectivity. When unsaturated motifs are present in the side chain, they diversify not only the shape but also the further modification of the amino acids. As such, it is encouraging to find that various types of olefin, including monosubstituted (**13**), 1,1/1,2-disubstituted (**14** and **15**) and trisubstituted (**16**) ones, as well as terminal (**17**) and internal (**18**) alkynes, can be integrated. Chains with multiple such motifs, including a diene derived from geraniol (**19**) and an enyne (**20**), are also compatible. Further transformations of these olefins and alkynes, such as coupling and oxidation reactions, are expected to generate amino acids of higher complexity. These functional groups have also been shown to facilitate chemical modification of peptides and proteins via metathesis[26] or click reactions[27].

The scope of functional groups stretches beyond unsaturated moieties. When a phenyl, indole or phthalimide was attached to the alkyl chain, unnatural analogues to phenylalanine (**21**), tryptophan (**22**) and ornithine (**23**) were formed, respectively. However, we note that the reduced enantioselectivity of **23** is proposed to result from the imide carbonyls that may interfere with the hydrogen bonding between the phosphoric acid and the enol intermediate. Malonic acids with a nitrile (**24**), acetal (**25**) or azide (**26**) group can also participate to give amino acids that inherit their versatile reactivity. Additionally, the acid catalyst operated smoothly on substrates with polyfunctionalized skeletons derived from cholic acid (**27**) and estrone (**28**) and the stereocontrol remained excellent despite their large sizes. We also demonstrated a route from *p*-methoxybenzyl ether (**29**) to proline (**32**) that is potentially general, to access natural or unnatural cyclic amino acids. More importantly, given the abundant reactivity of alcohol (**30**) and alkyl iodide (**31**), the pair of intermediates in the sequence are of great synthetic value to access other functionalized acyclic amino acids as well.

The synthesis of functionalized phenylalanines was also heavily investigated, given their prevalence in drugs and their role as a vessel to convey special functions to peptides and proteins (Table 1)[28]. We envisioned that the easy availability of assorted benzyl halides and their facile substitution reactions would help the asymmetric synthesis provide a reliable supply of these amino acids. Indeed, substituents

Fig. 3 | Synthesis of amino acids with diverse alkyl chains[a]. **a**, Malonate-based preparation of amino acids. Aminomalonic acids bearing the tailored benzamide (**Bz**^{7}) can be prepared on a large scale while the anchoring group is easily detached via hydrolysis to give amino acid hydrochloride salts (for example **5**). Amino acids of both configurations, such as (+)/(−)-**6**, can be obtained by using commercially available phosphoric acids. **b**, Preparation of alkyl-substituted amino acids. The chiral phosphoric acid is tolerant of primary and secondary alkyl groups of distinct shapes (**7**–**12**). **c**, Compatibility of the decarboxylation with unsaturated functional groups. Aminomalonic acids with unsaturated substituents, including diverse olefins (**13**–**16**), alkynes (**17** and **18**), dienes (**19**) and enynes (**20**), can all participate in the decarboxylation to give the corresponding amino acids. **d**, Accommodation of substrates with a large library of functional groups. The diversity of functional groups that can be introduced to amino acids is immense (**21**–**28**). Meanwhile, cyclic amino acids (for example **32**) are also accessible using the desymmetrization and subsequent derivatization. UAA, unnatural amino acid; Phe, phenylalanine; Trp, tryptophan; Orn, ornithine; Ser, serine; DDQ, 2,3-dichloro-5,6-dicyano-1,4-benzoquinone. [a]Unless noted otherwise, the decarboxylation was performed using aminomalonic acid (0.2 mmol) and **SPA** (0.02 mmol, 10 mol%) in 4 ml CPME at 80 °C (see Supplementary Section 7 for details). [b]The large-scale reaction was performed using 2.5 mol% (*R*)-**SPA** with 3.0 mmol aminomalonic acid slowly added via a syringe pump (see Supplementary Section 7 for details). [c]The yield and e.e. were obtained after recrystallization.

https://doi.org/10.1038/s41557-023-01362-3

of different shapes and electronic properties can all be carried along the route to corresponding phenylalanine derivatives (**34**–**44**). The diversity of functionality that can be introduced is ample. Besides the NMR-active fluorides (**34** and **42**) that are known to assist structural studies of proteins[29], both partners of the azide–alkyne cycloaddition (**45** and **48**) are compatible. In addition to an enolizable methyl ketone (**43**), the amino acid with a benzophenone motif (**46**) that was shown to enable enzymatic photocatalysis was also obtained[30,31]. The catalyst's tolerance of aryl nitrile and alkyne, as well as large terphenyl groups, allowed us to prepare privileged non-canonical fluorescent amino

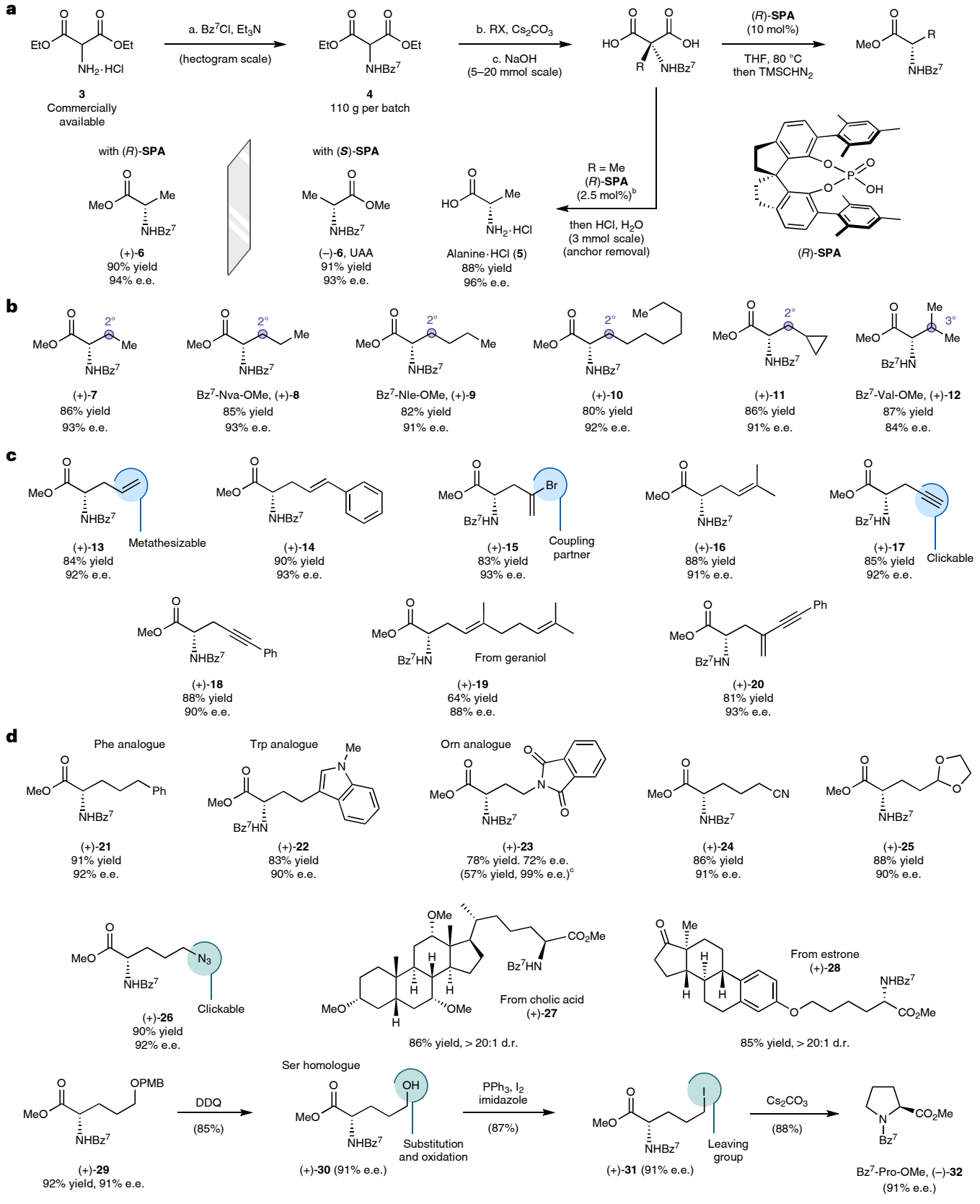

https://doi.org/10.1038/s41557-023-01362-3

Table 1 | Diverse preparation of functionalized phenylalanines

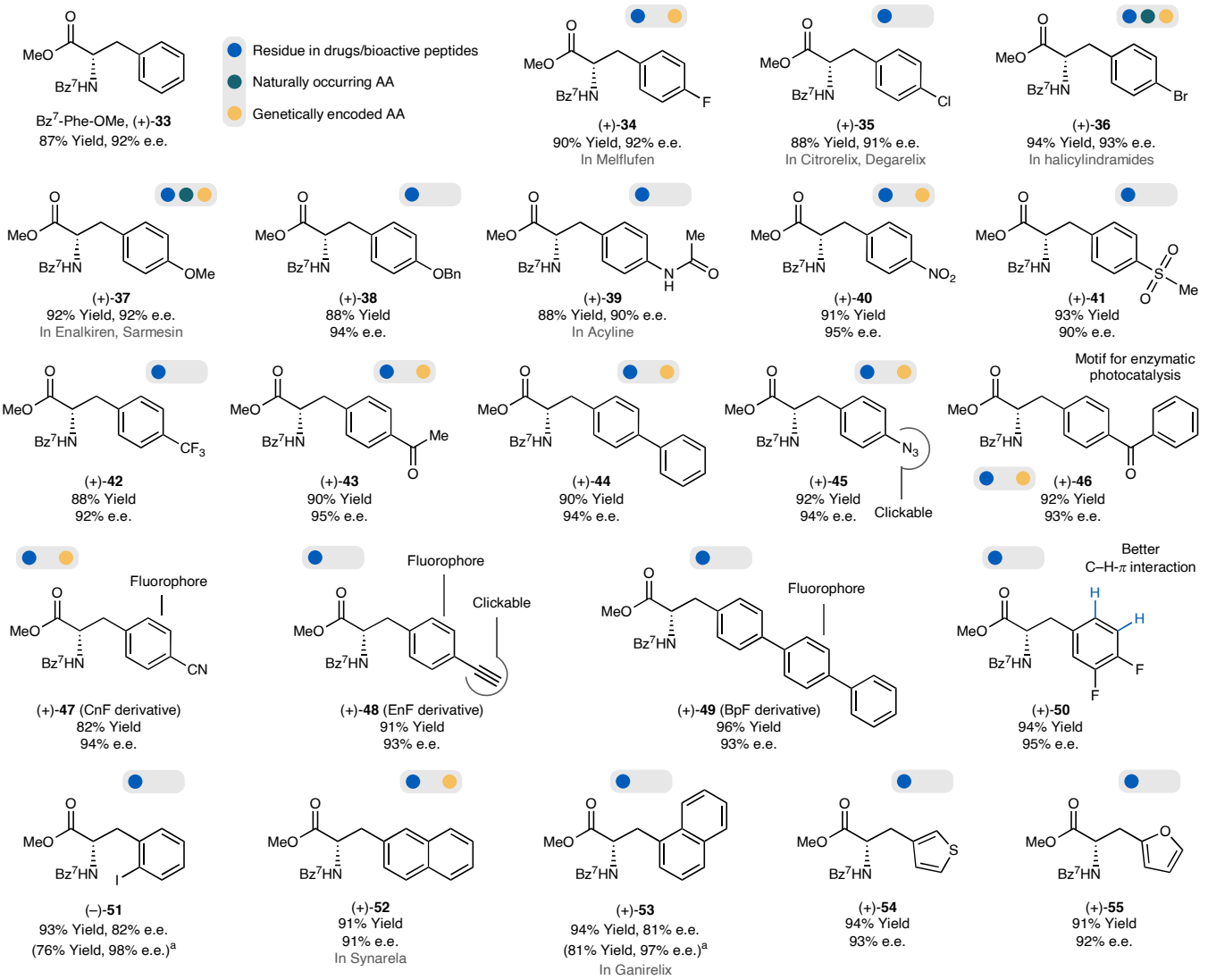

Unless noted otherwise, the decarboxylation was performed using aminomalonic acid (0.2 mmol) and **SPA** (0.02 mmol, 10 mol%) in 4 ml CPME at 80 °C (see Supplementary Section 7 for details). [a]The yield and e.e. were obtained after recrystallization. AA, amino acid; Bn, benzyl; CnF, cyanophenylalanine; EnF, ethynylphenylalanine; BpF, biphenylphenylalanine.

acids (**47**–**49**)[32]. Substitution patterns (**50** and **51**) and aromatic rings (**52**–**55**) other than these *para*-substituted phenyl groups (**34**–**49**) are equally well accommodated. We note that the couple of fluoro substituents in **50** were shown to reinforce C–H-π interactions within peptides by enhancing the acidity of aromatic hydrogens[33]. Meanwhile, the *ortho*-iodide motif (**51**) would help derivatize the phenylalanine core via cross coupling. Malonic acids with a naphthalene (**52** and **53**) or heterocycle (**54** and **55**) can also decarboxylate to give non-proteinogenic amino acids. Notably, slight reduction in stereocontrol can be observed when an *ortho* substituent is present (for example **51** and **53**), presumably due to the steric repulsion inside the catalyst pocket. Nevertheless, a simple recrystallization can enhance the enantiopurity without a large loss of yield.

Synthetic applications

Isotope-labelled amino acids are also accessible (Fig. 4a). These structures are in high demand given their diverse applications across several fields, including proteomics, pharmacokinetics and diagnostic radiology[34,35]. The decarboxylation-based synthesis can provide a modular approach that is highly flexible regarding the identity of isotopes and the targeted positions in amino acids. For example, the α-^{13}C and ^{15}N isotopes can be introduced via a condensation reaction to an oxime using labelled diethyl malonate or sodium nitrite, followed by reduction and benzoylation to α-^{13}C- or ^{15}N-**4**. On the other hand, the labelled side chains can be readily connected via substitution, as demonstrated by the preparation of d_3-**56**. Subsequently, all three labelled malonic acids were decarboxylated under acid catalysis to give enantio- and isotope-enriched alanines (**57**–**59**).

The alkyne- or azide-substituted amino acids generated in our study (**17**, **26**, **45** and **48**) can rapidly conjugate with biologically active cores, reflecting their potential application in discovering new amino acid- or peptide-based therapeutic agents (Fig. 4b). With a generic copper catalyst, the cycloaddition between the propargyl group in **17** and the azide motif in zidovudine proceeded smoothly (**60**). Another amino acid–antiretroviral drug conjugate was prepared from the azido-containing product (**45**) and propargyl-tethered lamivudine (**61**). Saccharides and amino acids can also connect using the same strategy (**62**).

Besides serving as anchoring groups, the 3-alkoxy-4-nitrobenz amides, once reduced to anilines, are often found in bioactive small molecules and peptides owing to their capability of imitating the α-helix conformation (**63**, Fig. 4c)[36]. Thus, a representative route towards these motifs was devised. Starting from the tailored aminomalonic acid (**64**), the asymmetric decarboxylation using (*S*)-**SPA**

https://doi.org/10.1038/s41557-023-01362-3

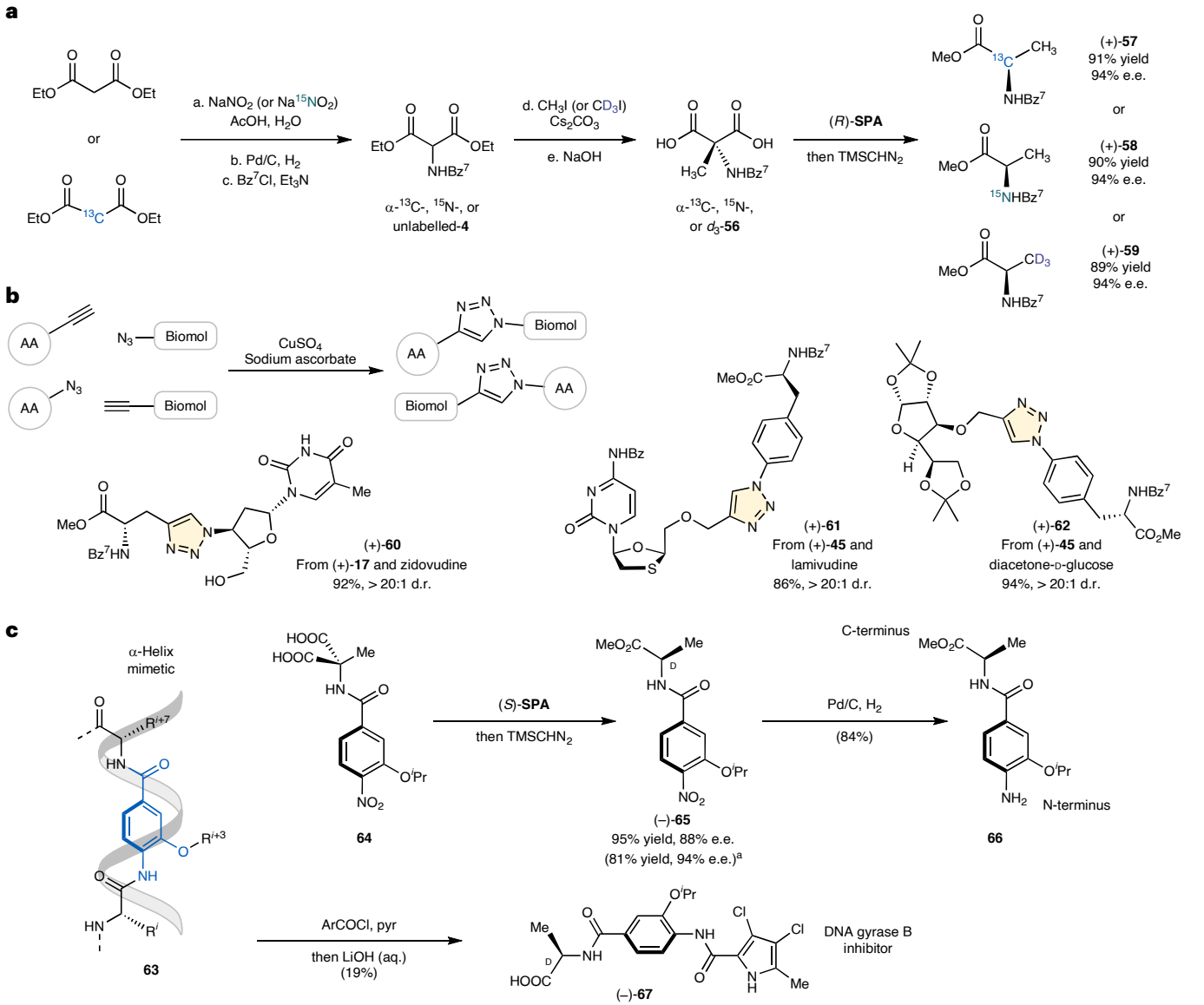

Fig. 4 | Representative application scenarios of the asymmetric malonic ester synthesis. a, Preparation of isotope-labelled amino acids. The bottom-up synthesis can be easily adapted to approach isotope-labelled amino acids. By using a unified synthetic sequence, we have shown that ^{13}C and ^{15}N isotopes can be introduced via an early-stage oxime formation, while the labelled side chains can be introduced via a later substitution. **b**, Click reactions using amino acids from the decarboxylation. Non-proteinogenic amino acids with an alkyne or azide motif that are prepared in our study can conjugate with other biomolecules rapidly using click chemistry. Both amino acid–antiretroviral drug and amino acid–saccharide conjugates were effortlessly prepared. **c**, Synthesis of an α-helix mimetic via the derivatization of the anchoring group. The 3-alkoxy-4-nitrobenzamide anchoring groups in our synthesis, once reduced to corresponding anilines, can serve as α-helix mimetics that frequently appear in bioactive peptides. As such, we have devised a decarboxylation/reduction sequence that synthesized a DNA gyrase B inhibitor (**67**) containing an unnatural alanine residue. [a]The yield and e.e. were obtained after recrystallization.

afforded an unnatural alanine motif (**65**) to serve as the C-terminus of the helix mimetic. Subsequently, the N-terminus was unmasked by a hydrogenation of the nitro group (**66**). The following acylation and ester hydrolysis produced DNA gyrase B inhibitor (**67**)[37].

Mechanistic and density functional theory studies

Analysis of initial rates (Fig. 5a) showed that the decarboxylation follows first-order kinetics in the malonic acid (**S6**) but is zeroth order with respect to the acid catalyst (**SPA**). Meanwhile, the lack of lag and exponential phases of product growth, as well as the constant enantioselectivity throughout the whole reaction (Supplementary Fig. 12), excluded the rare possibility of autocatalysis and autoinduction[38]. Overall, these kinetic data are consistent with a rate-determining self-decarboxylation followed by an enantio-determining phosphoric acid-mediated protonation. Indirect evidence of this scenario was also obtained (Fig. 5b). When a racemic half acid (**68**) was reacted with **SPA**, enantioenriched amino ester (**69**) was generated but the recovered half acid (**70**) remained racemic, indicating the irrelevance of the CO_2 extrusion step in the enantiocontrol.

Density functional theory (DFT) calculations were also carried out (Fig. 5c). Computational studies with substrate **S6** suggest that the self-decarboxylation via transition state **TS-1** requires a 1.2 kcal mol^{-1} lower energy barrier than that of the **SPA**-catalysed pathway through **TS-2S**. This demonstrates that the monomolecular self-decarboxylation pathway is more favoured. The lower energy barrier of self-decarboxylation can be attributed to the multifold hydrogen bonds in the bicyclic bridged-ring structure of **TS-1**. The amide group plays a critical role in promoting the decarboxylation by forming hydrogen bonds with the proton and renders **TS-1** distinct from conventional six-membered cyclic transition states (Supplementary Figs. 13 and 14). Moreover, the theoretical studies

https://doi.org/10.1038/s41557-023-01362-3

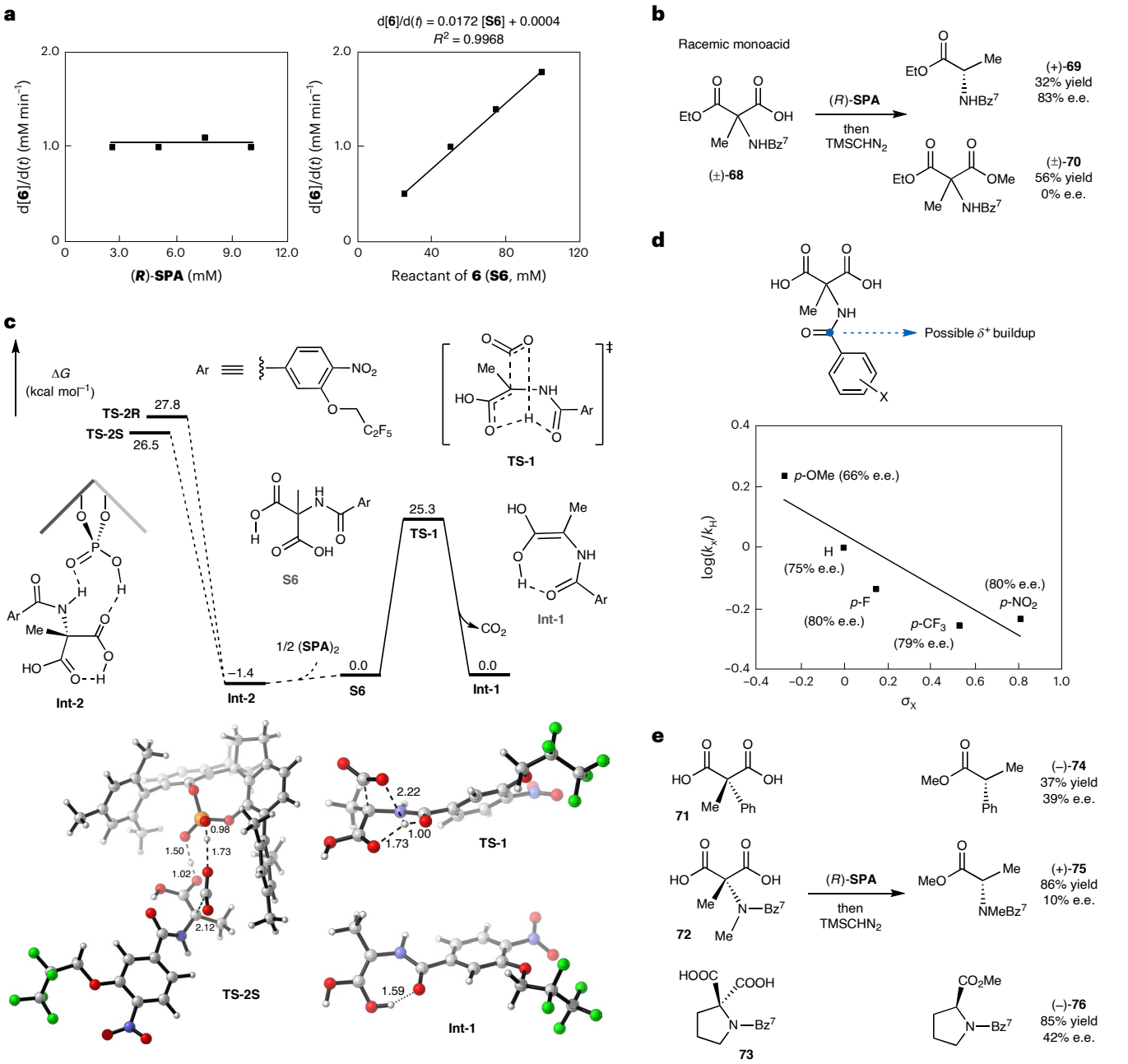

Fig. 5 | Mechanistic experiments and consideration. a, Kinetics of the decarboxylation. The decarboxylation expresses first-order kinetics in malonic acids and the initial rate is irrelevant to the concentration of chiral phosphoric acids. These data are consistent with a rate-determining CO_2 extrusion in the absence of acid catalysts. **b**, Decarboxylation of a monoacid. The reaction of malonic ester half acid (**68**) generated chiral decarboxylation products but recovered racemic reactants, which serves as indirect evidence for the pathway of self-decarboxylation followed by **SPA**-mediated protonation. **c**, Pathways of CO_2 extrusion. Computational study of the decarboxylation of **S6**. Both the **SPA**-mediated decarboxylation and the self-decarboxylation (without **SPA**) pathways are explored. The latter were proved to be more favoured, being consistent with mechanistic experiments. All energies were calculated at the M06-2X/6-311 + G(d,p)/SMD(CPME)//M06-2X/6-31 G(d,p) level of theory. **d**, Electronic effects of the anchoring group. The Hammett plot of the substituents on the anchoring group showed a negative ρ value, indicating a positive charge build-up during the CO_2 extrusion that is consistent with **TS-1**. **e**, Control experiments using three tailored malonic acids. The decreased enantioselectivity of the control experiments using three substrates (**71**–**73**) demonstrated the indispensable role of the secondary amide motif (that is $NHBz^7$) in enantiocontrol.

corroborate the experimental results that the decarboxylation is the rate-determining step as the following **SPA**-mediated protonation of enol **Int-1** has a lower energy barrier (see below, Fig. 6).

Notably, the DFT-optimized structure of **TS-1** also correlates with the findings from the screening of the amine anchoring group (Supplementary Fig. 5). As can be seen from the Hammett plot (Fig. 5d), the negative ρ value matches the hydrogen bonding between the amide carbonyl and the acid proton in **TS-1** that builds up positive charge at the *ipso* carbon. Besides tuning the rate of decarboxylation, these secondary benzamides also play a profound role in enantiocontrol (Fig. 5e). Control experiments using phenylmethylmalonic acid (**71**) or malonic acids with a tertiary amide motif (**72** and **73**) all gave largely inferior enantioselectivity, indicative of the indispensable participation of the secondary amide and its proton in the protonation inside the acid pocket.

DFT studies have witnessed a N–H···O hydrogen bond formed between the amide and the phosphoric acid in **SPA**-catalysed

https://doi.org/10.1038/s41557-023-01362-3

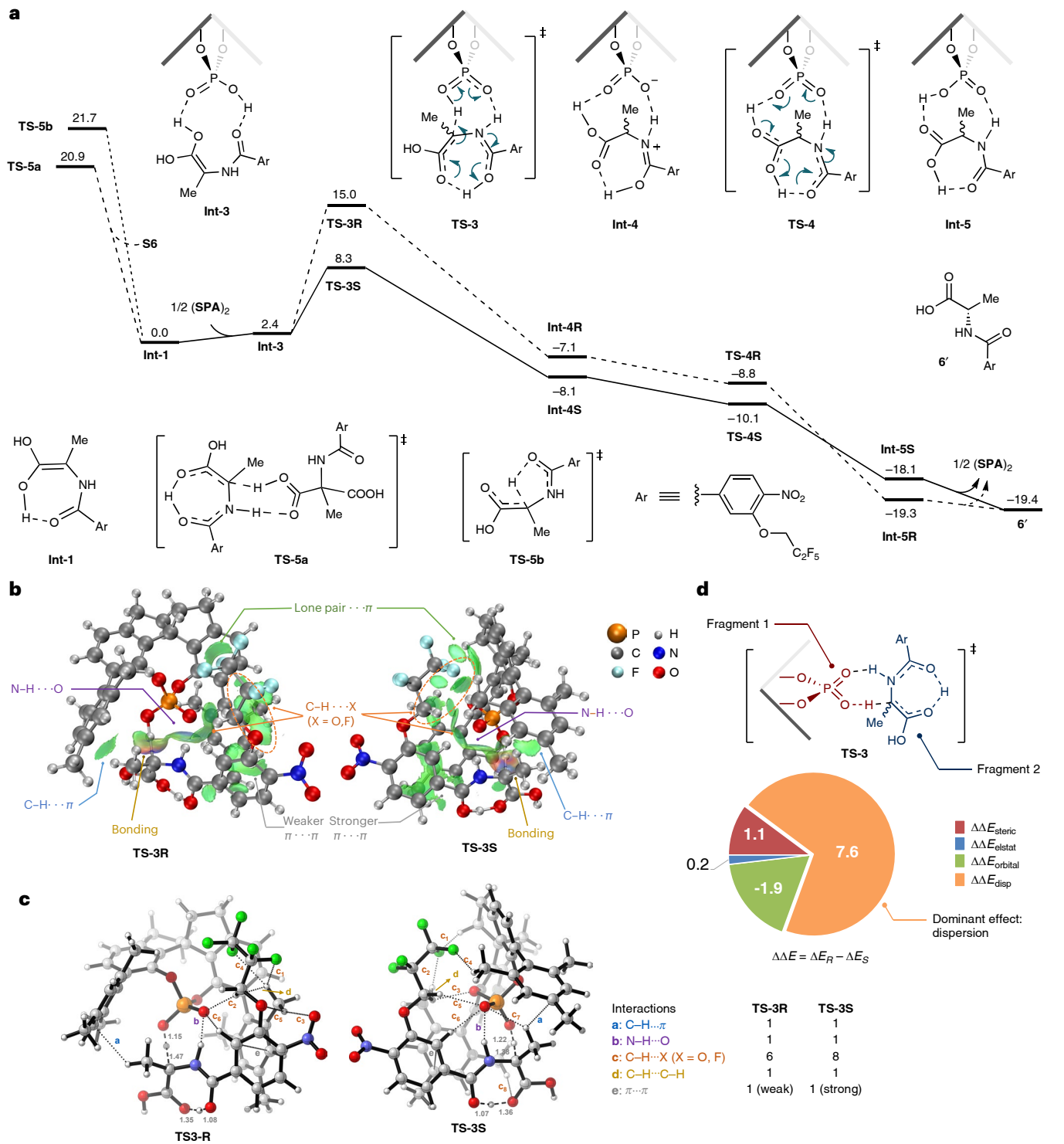

Fig. 6 | Origins of enantiocontrol and roles of the anchoring group. a, Free energy profile for the protonation. The **SPA**-mediated protonation through **TS-3** is determined to be the enantiocontrol step. **b**, IGMH analysis of the non-covalent interactions in **TS-3**. **TS-3S** has more hydrogen bonds and a stronger $\pi\cdots\pi$ interaction. **c**, Illustration of the numbers of major non-covalent interactions in enantiomers of **TS-3**. **TS-3S** has more dispersion forces and a stronger π–π interaction. **d**, Quantitative steric–electronic effect dissection using energy decomposition analysis based on absolutely localized molecular orbitals (ALMO-EDA) for the quantitative evaluation of ligand–substrate interactions on the enantioselectivity. The structure of the transition state was separated into the **SPA** fragment and the enol fragment in EDA. EDA calculations along the intrinsic reaction coordinate (IRC) of protonation were performed and the comparison of results between **TS-3R** and **TS-3S** at a C–H distance of 1.38 Å (observed in **TS-3S**) is shown here as an example to show the dominating role of the dispersion interaction. The corresponding structure of **TS-3R** with a C–H distance of 1.38 Å is obtained through IRC fitting based on cubic spline interpolation. See Supplementary Figs. 16–19 for details and extended explanation. The solvent effect is considered in an implicit manner using the solvation model density (SMD) solvation model (Supplementary Table 1 and Supplementary Fig. 19).

protonation transition states **TS-3S** and **TS-3R** (Fig. 6). This **SPA**-catalysed protonation pathway is kinetically favoured over the diacid **S6**-involved self-catalysis pathway (via **TS-5a**) and the intramolecular 1,4-hydrogen shift pathway (via **TS-5b**). More importantly, the **SPA**-catalysed protonation is proved to be the enantioselectivity-determining step and the following proton transfer through **TS-4** is barrierless (Fig. 6a). The computational results indicate that the activation free energy of **TS-3S** is 6.7 kcal mol^{-1} lower than that of **TS-3R**. The calculated energy difference suggests a much higher enantioselectivity than the experimental result (see above, Fig. 2, 94% e.e.). This may be due to the limitations of the implicit solvent model in fully simulating the steric and electronic properties of cyclopentyl methyl ether (CPME). Particularly, as ethereal CPME can catalyse proton transfer, the background protonation to racemic products may proceed more easily than the calculated barriers (that is of **TS-5a** and **TS-5b**) indicate.

To unravel the origin of enantiocontrol, the independent gradient model based on Hirshfeld partition (IGMH)[39] was used to study the non-covalent interactions between the **SPA** fragment and the enol fragment in both **TS-3S** and **TS-3R**. Various interactions between fragments are visualized in Fig. 6b and the numbers of interaction pairs are tabulated in Fig. 6c. A wider green surface between the aromatic rings, which represents a stronger $\pi\cdots\pi$ interaction, is observed in **TS-3S** between the electron-deficient benzene of the benzoyl anchoring group and the mesityl side arm of **SPA** (Fig. 6b). Moreover, two more pairs of C–H···X (X = O, F) interaction exist in **TS-3S** than in **TS-3R** (Fig. 6c). Notably, the electrostatically positive methylene and negative fluorine on the fluorinated alkoxy side chain (that is $-OCH_2CF_2CF_3$ of **Bz**^{7}) are spatially well contacted with the phosphoric acid. Particularly in the favoured transition state (**TS-3S**), the alkoxy chain on the anchoring group is closely embedded in an open pocket composed of a pair of methyl groups from mesityl substituents (c_2 and c_4), two oxygen atoms of the acid motif (c_3 and c_5) and a methylene group on the spirocyclic backbone (c_1) via five pairs of dispersive interaction (Fig. 6c). Though weaker than hydrogen bonds, the large number of these dispersion forces from the tailored benzoyl anchoring group (**Bz**^{7}) prove indispensable to the excellent level of enantiocontrol (see above, Fig. 2).

Furthermore, energy decomposition analysis based on absolutely localized molecular orbitals (ALMO-EDA)[40–46] was conducted to quantitatively evaluate the effect of different ligand–substrate interactions on the enantioselectivity. Comparison of the EDA results between **TS-3R** and **TS-3S** reveals that the more stabilizing dispersion interaction in **TS-3S** is the dominant factor controlling the enantioselectivity (Fig. 6d). According to previous studies exploring the nature of weak interactions, C–H···X interactions are claimed to be mainly from dispersion and the electrostatic effect[47] while $\pi\cdots\pi$ interaction is mainly a dispersion effect[48,49]. Thus, the ALMO-EDA result provides a quantitative complement for the qualitative IGMH analysis. Collectively, they clarify that the enantiocontrol stems from the more favoured dispersion induced by the stronger C–H···X and $\pi\cdots\pi$ interactions in the enol protonation step, primarily between the anchoring group and the acid catalyst.

Conclusion

We have demonstrated that a tailored benzamide motif can be installed on aminomalonic acids to induce multiple types of noncovalent interaction, including hydrogen bonds, π–π stacking and dispersion forces, with chiral phosphoric acids. The joint effects of these weak interactions proved indispensable to fix the enol intermediate inside the catalyst pocket and create a kinetically favoured pathway for protonation and thus allow an asymmetric decarboxylation to chiral amino acids. This study indicates that besides conventional catalyst modification, the use and structural optimization of anchoring groups on reactants could serve as an important tool to enhance catalyst–substrate interaction and thus unlock elusive reactivity and selectivity.

Online content

Any methods, additional references, Nature Portfolio reporting summaries, source data, extended data, supplementary information, acknowledgements, peer review information; details of author contributions and competing interests; and statements of data and code availability are available at https://doi.org/10.1038/s41557-023-01362-3.

References

1. Fehr, C. Enantioselective protonation of enolates and enols. *Angew. Chem. Int. Ed.* **35**, 2566–2587 (1996).
2. Duhamel, L., Duhamel, P. & Plaquevent, J. -C. Enantioselective protonations: fundamental insights and new concepts. *Tetrahedron* **15**, 3653–3691 (2004).
3. Mohr, J. T., Hong, A. Y. & Stoltz, B. M. Enantioselective protonation. *Nat. Chem.* **1**, 359–369 (2009).
4. Blanchet, J., Baudoux, J., Amere, M., Lasne, M.-C. & Rouden, J. Asymmetric malonic and acetoacetic acid syntheses – a century of enantioselective decarboxylative protonations. *Eur. J. Org. Chem.* 5493–5506 (2008).
5. Mohr, J. T., Nishimata, T., Behenna, D. C. & Stoltz, B. M. Catalytic enantioselective decarboxylative protonation. *J. Am. Chem. Soc.* **128**, 11348–11349 (2006).
6. Marinescu, S. C., Nishimata, T., Mohr, J. T. & Stoltz, B. M. Homogeneous Pd-catalyzed enantioselective decarboxylative protonation. *Org. Lett.* **10**, 1039–1042 (2008).
7. Morita, M. et al. Two methods for catalytic generation of reactive enolates promoted by a chiral poly Gd complex: application to catalytic enantioselective protonation reactions. *J. Am. Chem. Soc.* **131**, 3858–3859 (2009).
8. Mitsuhashi, K., Ito, R., Arai, T. & Yanagisawa, A. Catalytic asymmetric protonation of lithium enolates using amino acid derivatives as chiral proton sources. *Org. Lett.* **8**, 1721–1724 (2006).
9. Poisson, T., Oudeyer, S., Dalla, V., Marsais, F. & Levacher, V. Straightforward organocatalytic enantioselective protonation of silyl enolates by means of Cinchona alkaloids and carbxylic acids. *Synlett* 2447–2450 (2008).
10. Leow, D., Lin, S., Chittimalla, S. K., Fu, X. & Tan, C. -H. Enantioselective protonation catalyzed by a chiral bicyclic guanidine derivative. *Angew. Chem. Int. Ed.* **47**, 5641–5645 (2008).
11. Dai, X., Nakai, T., Romero, J. A. C. & Fu, G. C. Enantioselective synthesis of protected amines by the catalytic asymmetric addition of hydrazoic acid to ketenes. *Angew. Chem. Int. Ed.* **46**, 4367–4369 (2007).
12. Miyamoto, K. & Kourist, R. Arylmalonate decarboxylase—a highly selective bacterial biocatalyst with unknown function. *Appl. Microbiol. Biotechnol.* **100**, 8621–8631 (2016).
13. Wilding, M., Goodall, M. & Micklefield, J. in *Comprehensive Chirality* 402–409 (Elsevier, 2012).
14. Rueping, M., Kuenkel, A. & Atodiresei, I. Chiral Brønsted acids in enantioselective carbonyl activations – activation modes and applications. *Chem. Soc. Rev.* **40**, 4539–4549 (2011).
15. Min, C. & Seidel, D. Asymmetric Brønsted acid catalysis with chiral carboxylic acids. *Chem. Soc. Rev.* **46**, 5889–5902 (2017).
16. Akiyama, T. & Mori, K. Stronger Brønsted acids: recent progress. *Chem. Rev.* **115**, 9277–9306 (2015).
17. Maji, R., Mallojjala, S. C. & Wheeler, S. E. Chiral phosphoric acid catalysis: from numbers to insights. *Chem. Soc. Rev.* **47**, 1142–1158 (2018).
18. Knowles, R. R. & Jacobsen, E. N. Attractive noncovalent interactions in asymmetric catalysis: Links between enzymes and small molecule catalysts. *Proc. Natl Acad. Sci. USA* **107**, 20678–20685 (2010).

19. Neel, A. J., Hilton, M. J., Sigman, M. S. & Toste, F. D. Exploiting non-covalent π interactions for catalyst design. *Nature* **543**, 637–646 (2017).
20. Huang, D., Xu, F., Lin, X. & Wang, Y. Highly enantioselective Pictet–Spengler reaction catalyzed by SPINOL phosphoric acids. *Chem. Eur. J.* **18**, 3148–3152 (2012).
21. Okrasa, K. et al. Structure-guided directed evolution of alkenyl and arylmalonate decarboxylases. *Angew. Chem. Int. Ed.* **48**, 7691–7694 (2009).
22. Brunner, H. & Baur, M. A. α-Amino acid derivatives by enantioselective decarboxylation. *Eur. J. Org. Chem*. 2854–2862 (2010).
23. Lin, X., Wang, L., Han, Z. & Chen, Z. Chiral spirocyclic phosphoric acids and their growing applications. *Chin. J. Chem.* **39**, 802–824 (2021).
24. Xu, F. et al. SPINOL-derived phosphoric acids: synthesis and application in enantioselective Friedel–Crafts reaction of indoles with imines. *J. Org. Chem.* **75**, 8677–8680 (2018).
25. Rahman, A. & Lin, X. Development and application of chiral spirocyclic phosphoric acids in asymmetric catalysis. *Org. Biomol. Chem.* **16**, 4753–4777 (2018).
26. Messina, M. S. & Maynard, H. D. Modification of proteins using olefin metathesis. *Mater. Chem. Front.* **4**, 1040–1051 (2020).
27. Parker, C. G. & Pratt, M. R. Click chemistry in proteomic investigations. *Cell* **180**, 605–632 (2020).
28. Kim, C. H., Axup, J. Y. & Schultz, P. G. Protein conjugation with genetically encoded unnatural amino acids. *Curr. Opin. Chem. Biol.* **17**, 412–419 (2013).
29. Arntson, K. E. & Pomerantz, W. C. K. Protein-observed fluorine NMR: a bioorthogonal approach for small molecule discovery. *J. Med. Chem.* **59**, 5158–5171 (2016).
30. Trimble, J. S. et al. A designed photoenzyme for enantioselective [2+2] cycloadditions. *Nature* **611**, 709–714 (2022).
31. Sun, N. et al. Enantioselective [2+2]-cycloadditions with triplet photoenzymes. *Nature* **611**, 715–720 (2022).
32. Cheng, Z., Kuru, E., Sachdeva, A. & Vendrell, A. Fluorescent amino acids as versatile building blocks for chemical biology. *Nat. Rev. Chem.* **4**, 275–290 (2020).
33. Fujita, T. et al. Synthesis of a complete set of L-difluorophenylalanines, L-(F_2)Phe, as molecular explorers for the CH/π interaction between peptide ligand and receptor. *Tetrahedron Lett.* **41**, 923–927 (2000).
34. Mann, M. Functional and quantitative proteomics using SILAC. *Nat. Rev. Mol. Cell Biol.* **7**, 952–958 (2006).
35. Castellani, F. et al. Structure of a protein determined by solid-state magic-angle-spinning NMR spectroscopy. *Nature* **420**, 99–102 (2002).
36. Shaginian, A. et al. Design, synthesis, and evaluation of an α-helix mimetic library targeting protein–protein interactions. *J. Am. Chem. Soc.* **131**, 5564–5572 (2009).
37. Durcik, M. et al. New *N*-phenylpyrrolamide DNA gyrase B inhibitors: optimization of efficacy and antibacterial activity. *Eur. J. Med. Chem.* **154**, 117–132 (2018).
38. Walsh, P. J. & Kozlowski, M. C. in *Fundamentals of Asymmetric Catalysis* 330–374 (University Science Books, 2009).
39. Lu, T. & Chen, Q. Independent gradient model based on Hirshfeld partition: A new method for visual study of interactions in chemical systems. *J. Comput. Chem.* **43**, 539–555 (2022).
40. Horn, P. R., Mao, Y. & Head-Gordon, M. Defining the contributions of permanent electrostatics, Pauli repulsion, and dispersion in density functional theory calculations of intermolecular interaction energies. *J. Chem. Phys.* **144**, 114107 (2016).
41. Horn, P. R. & Head-Gordon, M. Polarization contributions to intermolecular interactions revisited with fragment electric-field response functions. *J. Chem. Phys.* **143**, 114111 (2015).
42. Horn, P. R., Mao, Y. & Head-Gordon, M. Probing non-covalent interactions with a second generation energy decomposition analysis using absolutely localized molecular orbitals. *Phys. Chem. Chem. Phys.* **18**, 23067–23079 (2016).
43. Qi, X., Kohler, D. G., Hull, K. L. & Liu, P. Energy decomposition analyses reveal the origins of catalyst and nucleophile effects on regioselectivity in nucleopalladation of alkenes. *J. Am. Chem. Soc.* **141**, 11892–11904 (2019).
44. Xi, Y. et al. Application of trimethylgermanyl-substituted bisphosphine ligands with enhanced dispersion interactions to copper-catalyzed hydroboration of disubstituted alkenes. *J. Am. Chem. Soc.* **142**, 18213–18222 (2020).
45. Mao, Y. et al. Consistent inclusion of continuum solvation in energy decomposition analysis: theory and application to molecular CO_2 reduction catalysts. *Chem. Sci.* **12**, 1398–1414 (2021).
46. Sengupta, A., Li, B., Svatunek, D., Liu, F. & Houk, K. N. Cycloaddition reactivities analyzed by energy decomposition analyses and the frontier molecular orbital model. *Acc. Chem. Res.* **55**, 2467–2479 (2022).
47. Emamian, S., Lu, T., Kruse, H. & Emamian, H. Exploring nature and predicting strength of hydrogen bonds: a correlation analysis between atoms-in-molecules descriptors, binding energies, and energy components of symmetry-adapted perturbation theory. *J. Comput. Chem.* **40**, 2868–2881 (2019).
48. Tsuzuki, S., Honda, K., Uchimaru, T., Mikami, M. & Tanabe, K. Origin of attraction and directionality of the π/π interaction: model chemistry calculations of benzene dimer interaction. *J. Am. Chem. Soc.* **124**, 104–112 (2002).
49. Carter-Fenk, K. & Herbert, J. M. Electrostatics does not dictate the slip-stacked arrangement of aromatic π–π interactions. *Chem. Sci.* **11**, 6758–6765 (2020).

Methods

General procedure for asymmetric decarboxylation

Q36 To an oven-dried 25 ml Schlenk tube was added the malonic acid (0.2 mmol, 100 mol%) and (*R*)-**SPA** (11.0 mg, 0.02 mmol, 10 mol%, purchased from Daicel Chiral Technologies and used as received). The flask was sealed with a rubber septum and evacuated/refilled with nitrogen three times. Then 4 ml CPME was added to the tube via a syringe under a nitrogen atmosphere and the reaction mixture was stirred at 80 °C for 5–20 h. After the reaction mixture was cooled to room temperature, 0.8 ml MeOH and 0.8 ml 2 M $TMSCHN_2$ (800 mol%) were added to the reaction mixture, which was stirred for an additional 1 h. The solvent was removed under reduced presure and the filtrate was purified by flash column chromatography (hexanes/ethyl acetate) to obtain the decarboxylation product.

Data availability

Q37 The data supporting the findings of this study are available within the paper and its Supplementary Information. Crystallographic data for compound (+)-**6** has been deposited at the Cambridge Crystallographic Data Centre (CCDC) under deposition no. CCDC 2206851. These data can be obtained free of charge from the CCDC (http://www.ccdc.cam.ac.uk/data_request/cif). Source data are provided with this paper.

Acknowledgements

We thank the University of Hong Kong for a start-up fund, the National Natural Science Foundation of China (22201222, X.Q.), the National Key R&D Program of China (2022YFA1505100, X.Q.), the Fundamental Research Funds for the Central Universities (2042022kf1038, X.Q.) and the Research Grants Council of Hong Kong (17304523, Z.H.). We acknowledge funding support from the Laboratory for Synthetic Chemistry and Chemical Biology under the Health@InnoHK Program launched by the Innovation and Technology Commission, the Government of HKSAR. J. Yip and B. Yan are acknowledged for mass spectrometry and NMR spectroscopy, respectively. X.Q. acknowledges the supercomputing system in the Supercomputing Center of Wuhan University.

Author contributions

Z.H. conceived and designed the project. W.-F.Z. carried out the experiments. W.-F.Z. and Z.H. analysed the experimental data. J.C. and X.Q. carried out the theoretical studies and analysed the data. All authors wrote the manuscript.

Competing interests

The authors declare no competing interests.

Additional information

Supplementary information The online version contains supplementary material available at https://doi.org/10.1038/s41557-023-01362-3.

Correspondence and requests for materials should be addressed to Xiaotian Qi or Zhongxing Huang.

Peer review information *Nature Chemistry* thanks Tian Lu and the other, anonymous, reviewer(s) for their contribution to the peer review of this work.

QUERY FORM

Manuscript ID	**[Art. Id: 1362]**
Author	**Wei-Feng Zheng**

AUTHOR:

The following queries have arisen during the editing of your manuscript. Please answer by making the requisite corrections directly in the e.proofing tool rather than marking them up on the PDF. This will ensure that your corrections are incorporated accurately and that your paper is published as quickly as possible.

Query No.	*Nature of Query*
Q1:	Please confirm you are happy with changes to the Abstract.
Q2:	Please confirm you are happy with the change to the sentence beginning 'Among asymmetric transformations that can...'.
Q3:	Please confirm you are happy with the change to the sentence beginning 'Moreover, when planar intermediates generated...'.
Q4:	Please confirm you are happy with the changes to the caption for Fig. 1 and that the added abbreviations 'Sub.' and 'Int.' are correct.
Q5:	Please check your article carefully, coordinate with any co-authors and enter all final edits clearly in the eproof, remembering to save frequently. Once corrections are submitted, we cannot routinely make further changes to the article.
Q6:	Note that the eproof should be amended in only one browser window at any one time; otherwise changes will be overwritten.
Q7:	Author surnames have been highlighted. Please check these carefully and adjust if the first name or surname is marked up incorrectly, as this will affect indexing of your article in public repositories such as PubMed. Also, carefully check the spelling and numbering of all author names and affiliations, and the corresponding author(s) email address(es). Please note that email addresses should only be included for designated corresponding authors, and you cannot change corresponding authors at this stage except to correct errors made during typesetting.
Q8:	You cannot alter accepted Supplementary Information files except for critical changes to scientific content. If you do resupply any files, please also provide a brief (but complete) list of changes. If these are not considered scientific changes, any altered Supplementary files will not be used, only the originally accepted version will be published.
Q9:	In the e.proof tool, the numbers for those compounds that will be deposited in PubChem do not appear bold, and the link is not visible. You do not need to amend this, they will appear correctly once published online.

QUERY FORM

Manuscript ID	**[Art. Id: 1362]**
Author	**Wei-Feng Zheng**

AUTHOR:

The following queries have arisen during the editing of your manuscript. Please answer by making the requisite corrections directly in the e.proofing tool rather than marking them up on the PDF. This will ensure that your corrections are incorporated accurately and that your paper is published as quickly as possible.

Query No.	*Nature of Query*
Q10:	Please check Figures for accuracy as they have been relabelled. Please markup minor changes in the eProof. For major changes, please provide revised figures. (Please note that in the eProof the figure resolution will appear at lower resolution than in the pdf and html versions of your paper.)
Q11:	If applicable, please ensure that any accession codes and datasets whose DOIs or other identifiers are mentioned in the paper are scheduled for public release as soon as possible, we recommend within a few days of submitting your proof, and update the database record with publication details from this article once available.
Q12:	Please confirm you are happy with the change to the sentence beginning 'These favoured conformations...'.
Q13:	Please confirm you are happy with the change to the sentence beginning 'Their stabilization effects still fall short...'.
Q14:	Please confirm you are happy with the changes to the caption for Fig. 2. Please add descriptions of the various parts of the figure to the caption and also explain the table. Please also define 'TMS'.
Q15:	Please confirm you are happy with the changes to the caption for Fig. 3. Note that citations to the Supplementary Information have been formatted for style. Please define Nva, NIe, VaI, PMB and Pro.
Q16:	Please confirm you are happy with the changes to the sentence beginning 'As proposed, enhancements in enantioselectivity...'.
Q17:	Please confirm you are happy with the change to the sentence beginning 'Indeed, a para-nitro group (Bz1)...'.
Q18:	Please confirm you are happy with the change to the sentence beginning 'The final and critical increment of enantiocontrol...'. Please clarify what you mean by 'increment'.
Q19:	Please confirm you are happy with the change to the sentence beginning 'When a larger-scale decarboxylation under a lower catalyst loading...' and also the change to the following sentence.

QUERY FORM

Manuscript ID	**[Art. Id: 1362]**
Author	**Wei-Feng Zheng**

AUTHOR:

The following queries have arisen during the editing of your manuscript. Please answer by making the requisite corrections directly in the e.proofing tool rather than marking them up on the PDF. This will ensure that your corrections are incorporated accurately and that your paper is published as quickly as possible.

Query No.	*Nature of Query*
Q20:	Please confirm you are happy with the change to the sentence beginning 'We note that while reducing the SPA loading...'.
Q21:	Please confirm you are happy with the change to the sentence beginning 'The approach also tolerates more...'.
Q22:	Please confirm you are happy with the change to the sentence beginning 'When a phenyl, indole or phthalimide...' as well as the changes to the following sentence.
Q23:	Please confirm you are happy with the changes to the sentence beginning 'We note that the couple of fluoro substituents...'.
Q24:	Please confirm you are happy with the change to the sentence beginning 'Notably, slight reduction in stereocontrol can be observed...'.
Q25:	Please confirm you are happy with the changes to the caption for Fig, 4, particularly for panel **b**. Please define 'pyr'.
Q26:	Please confirm you are happy with the change to the sentence beginning 'With a generic copper catalyst, the cycloaddition between...'.
Q27:	Please confirm you are happy with the change to the sentence beginning 'When a racemic half acid 68...'.
Q28:	Please confirm you are happy with the changes to the caption for Fig.5.
Q29:	Please confirm you are happy with the change to the sentence beginning 'This demonstrates that the monomolecular...'.
Q30:	Please confirm you are happy with the changes to the caption for Fig. 6. Please define the 'E' values in panel d (E_disp etc.).

QUERY FORM

Manuscript ID	**[Art. Id: 1362]**
Author	**Wei-Feng Zheng**

AUTHOR:

The following queries have arisen during the editing of your manuscript. Please answer by making the requisite corrections directly in the e.proofing tool rather than marking them up on the PDF. This will ensure that your corrections are incorporated accurately and that your paper is published as quickly as possible.

Query No.	*Nature of Query*
Q31:	Please confirm you are happy with the change to the sentence beginning 'This SPA-catalysed protonation pathway...'.
Q32:	Please confirm you are happy with the changes to the sentence beginning 'This may be due to the limitations of...' as well as the change to the following sentence.
Q33:	Please confirm you are happy with the change to the sentence beginning 'Various interactions between fragments...'.
Q34:	Please confirm you are happy with the changes to the sentence beginning 'According to previous studies exploring...'.
Q35:	Please confirm you are happy with all changes to the 'Conclusion' section.
Q36:	Please confirm you are happy with all changes to the 'Methods' section.
Q37:	We have merged the source data files for Fig. 5 into a single file. Please confirm that the contents are correct. Please also check that the CCDC ID is correct as this gave an error.
Q38:	For ref. 13 please add editors and edition number.